LATVIAN JOURNAL OF PHYSICS AND TECHNICAL SCIENCES
2017, N 1

DOI: 10.1515/lpts-2017-0007

NANOINDENTATION RESPONSE ANALYSIS OF THIN FILM SUBSTRATES-I: STRAIN GRADIENT-DIVERGENCE APPROACH

U. Kanders[1], K. Kanders[2]

[1]Institute of Mechanical Engineering,
Riga Technical University,
6 Ezermalas Str., LV-1006, Riga, LATVIA
uldis.kanders@gmail.com
[2]Institute of Neuroinformatics, University & ETH of Zurich
190 Winterthurerstr., CH-8057 Zurich, SWITZERLAND
kkanders@ini.phys.ethz.ch

Nanoindentation is a widely-used method for sensitive exploration of the mechanical properties of micromechanical systems. We derive a simple empirical analysis technique to extract stress-strain field (SSF) gradient and divergence representations from nanoindentation data sets. Using this approach, local SSF gradients and structural heterogeneities can be discovered to obtain more detail about the sample's microstructure, thus enhancing the analytic capacity of the nanoindentation technique. We demonstrate the application of the SSF gradient-divergence analysis approach to nanoindentation measurements of bulk silicon.

Keywords: *elastic-plastic deformation, nanoindentation, strain gradient plasticity, stress-strain field, true hardness, true elastic modulus*.

1. INTRODUCTION

Nanoindentation is a powerful experimental technique to characterise the mechanical properties of small volume samples, such as thin films and coatings, subsurface layers of bulk solids or biological materials such as bone, tooth enamel and even viruses [1]–[5]. The measurement usually has high variability at shallow penetration depths. Consequently, the material hardness and elastic modulus are commonly calculated from data averaged over around ten or more single indentation tests at depths exceeding at least 200–300 nm. Preferably the measured variable has then approached some stable steady state value that corresponds to the so-called material bulk property, often measured by the micro- or macro-indentation techniques. However, there are also situations when a steady state nanoindentation response at increasing penetration depth cannot be generally achieved or expected. For example,

it is not always possible to observe a stationary plateau in the nanoindentation measurement of hardness or elastic modulus in thin film samples when a strong reverse indentation size effect is present [6], [7] or when the sample substrate is influencing the experiment [8], [9]. Similarly, the subsurface layer of bulk solids is usually highly heterogeneous, which might preclude the apparent hardness and/or elastic modulus to approach a stationary value [3].

In this study, we derived a simple empirical approach to extract the local stress-strain field (SSF) gradient and divergence representations from the nanoindentation experiment dataset. The strain-gradient representations, in principle, facilitate the discovery of weak structural heterogeneities, indicating, for example, interfaces between mechanically distinct local microzones within the near surface region or work hardening and softening processes induced underneath the indenter. Furthermore, the SSF gradient representations allow defining an analytic criterion for determining the values of true hardness and true elastic modulus. We show the strain gradient-divergence analysis results of the nanoindentation response of a bulk solid silicon sample. Further application to bulk samples of various thin film substrates, such as different types of bearing and tooling steels as well as fused silica, is presented in the second part of the present research [10].

2. METHODS

2.1. Derivation of the Stress-Strain Field Gradient and Divergence Representations

In the nanoindentation experiment, each new indentation increment causes a mechanical shock that generates an elastic-plastic deformation wave, which propagates throughout the sample and fades when the system is relaxed. As a result, a stress-strain tensor field of restoring forces is induced periodically in the sample. In this section, we propose that useful information about the SSF can be extracted from the nanoindentation measurement, namely the representations of SSF gradient and divergence. The analysis technique derived below builds upon the strain gradient plasticity theory where the stress-strain relationship at any given point is considered in the context of deformation events in the long range vicinity of that point [11], [12].

In the expanding cavity model, a heavily deformed hydrostatic core encases the indenter tip as deep and wide as the contact radius, a_c. The hydrostatic core is surrounded by superimposed hemispherical plastic and elastic deformation zones [1], [13]. The contact radius differs from penetration depth, h, by a constant factor, e.g., about 3 times ($a_c \approx 2.79h$) in the case of the sharp Berkovich indenter. However, when using logarithmic coordinates instead of linear ones for the penetration depth, the choice between $\log(h)$ or $\log(a_c)$ only shifts the function plot along h-axis and does not change its form. This reason and the fact that the peak pressure between the core and the plastic deformation zone is quite diffuse allows us to simplify the analysis of the SSF and use h as an independent variable instead of a_c. The hydrostatic core is considered an incompressible, homogeneous extension of the indenter tip that transduces the applied test load, $P(h)$, into the SSF. The indented system resists to further elastic-plastic deformation and compensates the applied test load

according to Newton's third law. There is no such probe to measure directly the SSF components at each point $R(x,y,z \geq h)$ throughout the sample during a nanoindentation experiment, but one can measure the integrated echo of the SSF on the interface between the core and the plastic deformation zone $R(z = h)$ as the restoring force $F(h) = -P(h)$, or the total stress $\sigma_t(h) = F(h)/(2\pi h^2)$. The force field in the X-Y plane at each $z=h$ here and thereafter is assumed to be central symmetric. Therefore, all the restoring force components F_{xy} in the infinite X-Y plane compensate each other resulting in zero value. Thus, the only $F_z=F(h)$ component resists to loading force $P(h)$ exerted by the indenter. Note that total stress $\sigma_t(h)$ can be interpreted as the potential deformation energy density function of SSF. This allows us to introduce a generalized quantity, the SSF potential function $U(h)$ that is proportionally related to the stored potential deformation energy. Application of the nabla operator to $U(h)$ creates a gradient field $\nabla U(h)$. Strong gradient of the SSF at a point $R(x,y,z = h)$ is evidence that the indented system is highly heterogeneous in a short-range vicinity of this point, whereas a weak or zero gradient is a good sign that the system is homogeneous even in a long-range vicinity. We define the normalized gradient of the generalized potential function $U(h)$ as

$$U'(h) \equiv \frac{h}{U(h)} \nabla U(h) \tag{1}$$

The gradient $U'(h)$ is a very simplified force vector field (here and thereafter a vector sign is omitted due to simplicity), which represents to some extent the much more complex actual stress-strain tensor field beneath the loaded indenter. In turn, we define the SSF divergence as the divergence of the $U'(h)$ vector field by

$$U''(h) \equiv \nabla U'(h). \tag{2}$$

Divergence is closely related to stress-strain field flux density – the amount of stress-strain flux entering or leaving a given point $R(x,y,z = h)$. $U''(h)$ tells us at which h values the interface between the hydrostatic core and the plastic deformation zone acts as a stress-strain flux source or sink. It is easy to see that positive divergence means that the interface acts as a stress-strain flux source resulting in strain hardening effect, whereas negative divergence means that the interface acts as a stress-strain flux sink resulting in strain softening effect.

The total stress, $\sigma_t(h)$, can be broken down into elastic, $\sigma_e(h)$, and plastic, $\sigma_p(h)$, components, and each of these can be further separated into normal and shear stresses. Therefore, we can describe the total stress or the total potential strain energy density of the SSF as a superposition of the elastic normal, $\sigma_{en}(h)$, the elastic shear, $\sigma_{e\tau}(h)$, the plastic normal, $\sigma_{pn}(h)$, the plastic shear, $\sigma_{p\tau}(h)$, stress components. It remains to be shown how to link these stress components to the appropriate experimental datasets obtained during a nanoindentation experiment. Knowing the area of the interface between the hydrostatic core and the plastic deformation zone, one can calculate the average total stress:

$$\sigma_t(h) = \frac{F(h)}{2\pi h^2} = \frac{-P(h)}{2\pi h^2} \Rightarrow \sigma_t(h) \propto \frac{-P(h)}{h^2} \tag{3}$$

We assume that the elastic and plastic stress fields are superimposed and have a joint interface with the core [14]. The total elastic stress, $\sigma_e(h)$, can be evaluated using the harmonic contact stiffness, $S(h)$, experimental dataset:

$$\sigma_e(h) = \frac{S(h)h}{2\pi h^2} = \frac{S(h)}{2\pi h} \Rightarrow \sigma_e(h) \propto \frac{S(h)}{h} \tag{4}$$

Elastic normal stress component is represented by the well-known relationship containing elastic modulus, $E(h)$: $\sigma_{en}(h) = E(h)\varepsilon_{en}$, where ε_{en} is the elastic normal strain. In the nanoindentation experiment, the increment δh is changed progressively so that the incremental strain, $\varepsilon_{en} = \delta h/h$, is usually kept almost constant. Step by step indentation with a constant incremental strain has the advantage of logarithmically scaling the data density so that there are equal amounts of data at low and high loads. Therefore, we can treat the incremental strain as a constant variable and simplify to

$$\sigma_{en}(h) \propto E(h). \tag{5}$$

The total plastic stress component can be represented by hardness, $H(h)$:

$$\sigma_p(h) \propto H(h). \tag{6}$$

Using the definition of SSF gradient from Eq. 1, we derived the specialised elastic-plastic strain gradients from Eqs. 3–6:

$$\begin{aligned} P'(h) &\equiv \frac{h}{P(h)}\frac{dP(h)}{dh} - 2 \\ S'(h) &\equiv \frac{h}{S(h)}\frac{dS(h)}{dh} - 1 \\ E'(h) &\equiv \frac{h}{E(h)}\frac{dE(h)}{dh} \\ H'(h) &\equiv \frac{h}{H(h)}\frac{dH(h)}{dh} \end{aligned} \tag{7}$$

where $P'(h)$ represents total strain gradient, $S'(h)$ represents elastic total strain gradient, $E'(h)$ represents elastic normal strain gradient, and $H'(h)$ represents plastic total strain gradient induced beneath the indenter. In the rest of the text, we will refer to these functions as the corresponding strain gradients instead of strain gradient representations because they differ by a constant factor only. In an analogous way, we also derive the specialised total, $P''(h)$, elastic total, $S''(h)$, elastic normal, $E''(h)$, and plastic total, $H''(h)$ divergences using the definition in Eq. 2:

$$\begin{aligned} P''(h) &\equiv \nabla P'(h), \\ S''(h) &\equiv \nabla S'(h), \\ E''(h) &\equiv \nabla E'(h), \\ H''(h) &\equiv \nabla H'(h). \end{aligned} \tag{8}$$

In practice, we estimated the gradient and divergence representations by calculating the analytic derivative of a polynomial fit to the measurement data and gradient representation, respectively. The fit was applied to a sliding window of $2m+1$ points. Results with 1st (i.e., linear) and 2nd order fits were already found to be satisfactory, with m = 8, 9 or 10 providing the optimal window lengths indicated by robust accuracy of the fits (generally, R-squared value about 0.9 at shallow and greater than 0.99 at deeper indenter penetration depths). The differences between the linear and 2nd order fit were less than 2 % of peak amplitude at very shallow penetration depths (h < 32 nm). In the present paper, we present the results obtained using a linear fit with m=8. The exact length of the window did not affect the results strongly.

2.2 Experimental Details

The instrumented depth sensing nanoindentation experiments were performed on silicon substrates Si(100). The sample (20x20x0.381 mm^3) was cut off from silicon wafer. Surface roughness parameter RMS of the sample was lower than 1 nm.

G200 Nano Indenter (Agilent, USA) with a sharp Berkovich diamond indenter (tip radius < 20 nm) was used. Measurements were made in the continuous stiffness measurement (CSM) mode [15] and in the BASIC mode at different values of the maximum load. The load capability of the Nano Indenter G200 can reach up to 600 mN with the standard option. The hardness and elastic modulus of the samples were calculated by the MTS TestWorks 4 software using Oliver-Pharr method [16].

3. RESULTS AND DISCUSSION

We performed nanoindentation experiments on different bulk samples often used as substrates for thin film coatings: faceted and polished tooling and bearing steel samples, glass and fused silica slides, and silicon wafers. Here, we give a brief demonstration of the indentation response analysis from the Si(100). Perfectly smooth Si(100) sample was chosen as a material with single crystal structure and well-known mechanical properties to validate the strain gradient-divergence approach developed above. Further results on the steel samples and fused silica, as well as a quantitative treatment of the oscillations are provided in the second part of the present research [10].

3.1 SSF Gradient and Divergence in Bulk Silicon

Traditionally in the nanoindentation analysis, the measurements of several single indentation tests are averaged out to estimate the mechanical properties of the material. Usually this is performed automatically by the software of the nanoindentation apparatus. However, at shallow penetration depths the averaged estimations commonly have a rather high variability (standard deviation), thus precluding the observations of specific peculiarities of the sample subsurface layer. Therefore, the analysis of single indentation test datasets is necessary before any automatic data averaging procedure. We carried out 8 single indentation tests on the crystalline Si(100)

sample, which we first analysed individually and then we applied the analysis to the averaged measurements as well (we observed that as little as 6 tests had already been sufficient to reliably calculate average material mechanical properties such as hardness, elastic modulus, storage modulus, loss modulus and complex modulus among others). Figure 1(a) shows a typical example of a single measurement in the CSM mode when hardness, H, and elastic modulus, E, were measured as a function of indentation depth, h, continuously along the characteristic of load-displacement, P-h. The relatively smooth P-h curve is contrasted with the corresponding total SSF gradient, P'-h, curve, which was derived using the approach introduced in Methods Section. The analysis revealed quasi-regular oscillations of the SSF gradient that could be observed already starting from 16 nm penetration depth. Initial fluctuations can also be observed for $h < 16$ nm, which were, however, interrupted by nanoindentation induced phase transformation [17], [18] when the indenter reached penetration depths of 13–15 nm. This clearly visible breach in the P'-h curve oscillations would be difficult to discover in the load-displacement curve. Phase transition at 13-15 nm in silicon is most likely related to structural changes from the cubic diamond structure of silicon (Si-I) to its amorphous metallic phase (Si-II) under small indentation load. This (Si-I)|(Si-II) phase transformation manifested by the P'-h curves was present in all the single indentation tests of silicon that we performed. The oscillations of SSF divergence, P''-h, also convincingly revealed this (Si-I)|(Si-II) phase transformation (Fig. 1(b)). The non-monotonic behaviour due to complicated plastic deformation events underneath the indenter is also manifested by distinct superstructure of the moving average trendline of the P'-h curve (not shown). Depending on maximum load and loading-unloading rate parameters one can observe complicated structural changes in cubic Si(100) [17], [18], beginning with the single diamond crystal structure (Si-I), amorphous metallic phase (Si-II), polycrystalline phase (Si-III) and ending with a mixed structure of nanocrystalline phase (Si-XII) encaged by amorphous a-Si phase.

The moving average trendline of the SSF gradient, P'-h, curve allows dividing the displacement h-axis into several intervals such as 2–13 nm, 16–38 nm, 40–58 nm, 60–86 nm, 116–288 nm and 500–900 nm, which could be attributed to some extent to the above-mentioned phase transformations. Undoubtedly, further structure and chemical bonding sensitive investigations such as selected area diffraction (SAD), Raman spectroscopy and XPS among others are needed to understand the nanoindentation behaviour of Si, including structural inhomogeneities in the subsurface layer.

Oscillations of the total SSF divergence, P''-h, total plastic SSF divergence, H''-h, and elastic normal SSF divergence, E''-h, shown in Fig. 1(b-d) highlight the fine structure of the plastic deformation mechanisms occurring underneath the loaded indenter during a single indentation test. The P''-h, H''-h and E''-h curves for all tests demonstrated quasi-regular oscillations around the abscissa where at each intersection point the divergence amplitude changed its sign. Positive amplitude means that the indented sample underneath the indenter within the interface between the encasing hydrostatic core and plastic zone undergoes a strain (work) hardening plastic deformation whereas negative divergence amplitude indicates different plastic deformation leading to strain (work) softening effects. Divergence oscillation am-

plitude quickly decreased as the penetration depth increased, indicating that material bulk properties began to dominate over the subsurface layer influence at larger penetration depths. The small amplitude of *P″-h* curve at h > 250 nm manifested that the steady state region was reached where indents became self-similar when indenter load was increasing. Meanwhile, the hardness-displacement, *H-h*, curve reached the saturation plateau but the plastic SSF gradient, *H′-h*, had very low-amplitude oscillations around zero (not shown). The oscillations of *H″-h* and *E″-h* curves were out of phase (Fig. 1(c)), which was in good agreement with the general nature of the elastic-plastic deformation events. Note that any discrete plastic deformation event has its own early elastic phase manifested here by the positive elastic SSF divergence (*E″(h)* > 0). Elastic phase can happen only up to the point where the elastic limit is not yet exceeded. After the local yield point is reached, the elastic strain triggers the corresponding plastic one.

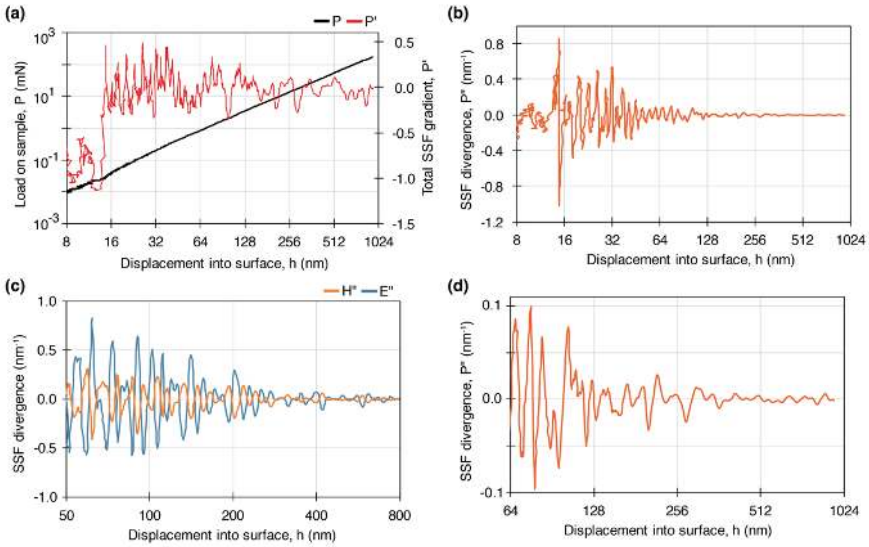

Fig. 1. Total stress-strain field gradient and divergence oscillations of the single indentation test in the Si(100) sample: **(a)** A typical example of the load-displacement, *P-h*, curve (black) and the total SSF gradient, *P′-h*, curve (red) obtained from a single indentation test in the CSM mode; **(b)** Total SSF divergence oscillations obtained from the same measurement; **(c)** Plastic normal (*H″-h* curve, orange) and elastic normal (*E″-h* curve, blue) SSF divergence oscillations calculated from the same measurement; **(d)** Close-up of the total SSF divergence low amplitude oscillations from (b) at greater penetration depths.

3.2 SSF Gradient-Divergence Analysis of the Averaged Dataset

The SSF gradients calculated from the averaged load-displacement, *P-h*, stiffness-displacement, *S-h*, hardness-displacement, *H-h*, and elastic modulus-displacement, *E-h*, curves (Fig. 2) were much smoother than the ones obtained from individual single measurements; the oscillations were much less salient. Similarly, the oscillations of the averaged SSF divergence could still be detected albeit they were markedly smaller in amplitude compared to the single indentation tests (not shown; see also Ref. 10). The smoothening occurred due to the averaging because the oscil-

lations of the single indentation tests were stochastically shifted in phase (along the *h*-axis) with respect to each other transforming the averaged SSF gradients into more quiet peak-valley system. However, it was still possible to detect less subtle fluctuations in the SSF gradients despite the averaging: each of the averaged SSF gradient curves demonstrated a sequence of peaks-valleys (see Fig. 2). The system of peaks-valleys in the averaged SSF gradient curves could be likely attributed to interfaces between mechanically distinct local microzones within the sample.

3.3 Calculation of True Hardness and True Elastic Modulus

One of the first questions that arise during the nanoindentation experiment is how to extract true hardness and true elastic modulus from raw indentation data such as the *P-h* and *S-h* curves or even from *H-h* and *E-h* curves calculated by Oliver-Pharr method [15] when they all are functions of the displacement within the whole displacement range. In this context, the averaged SSF gradients *H'-h* and *E'-h* play a significant role. In accordance with strain gradient plasticity concept, one should search for some special H_t- and E_t-points on the *H-h* and *E-h* curves where the corresponding strain gradients *H'-h* and *E'-h* intersect the displacement *h*-axis or approach it as close as possible, i.e., to find the deepest valley on the *H'-h* and *E'-h* curves if such intersection h_t-points do not exist. In the absence of the SSF gradients (i.e., zero gradient) *H-h* and *E-h* curves in the vicinity of these h_t-points may become state functions where apparent hardness, *H*, or elastic modulus, *E*, does not differ from the true hardness, H_t, or true elastic modulus, E_t. Following this approach, the true values of the hardness and elastic modulus could be read out from Fig. 2(c,d) as H_t = 12.3 GPa and E_t = 221.5 GPa, respectively.

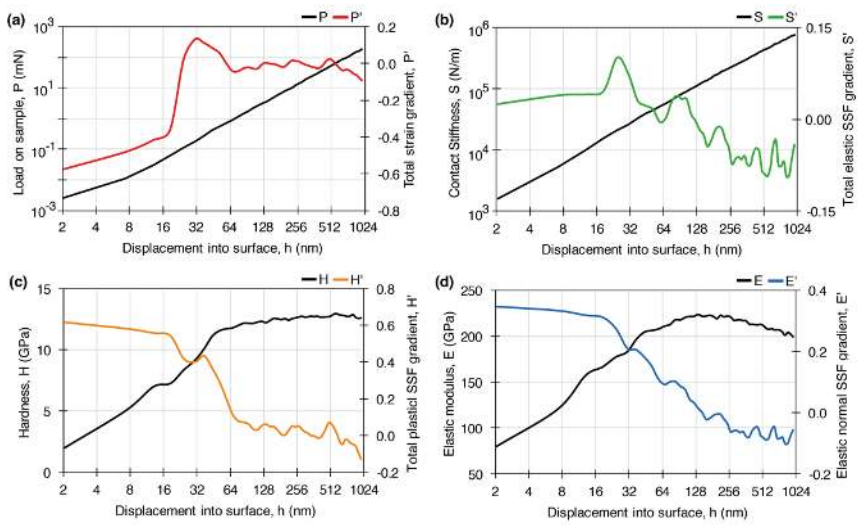

Fig. 2. Primary indentation characteristics and their corresponding SSF gradients calculated from the averaged datasets of the Si(100) sample (n=8 tests): **(a)** Load-displacement, *P-h*, curve and total SSF gradient-displacement, *P'-h*, curve; **(b)** Stiffness-displacement, *S-h*, and total elastic SSF gradient-displacement, *S'-h*, curve; **(c)** Hardness-displacement, *H-h*, and total plastic SSF gradient-displacement, *H'-h*, curve; **(d)** Elastic modulus-displacement, *E-h*, curve and elastic normal SSF gradient-displacement, *E'-h*, curve.

Some weak SSF gradient fluctuations up and down the h-axis may occur when the indentation steady state is reached. In such a case, several h_{ti}-points may appear instead of one critical h_t-point. If the h_{ti}-points are closely placed to each other and corresponding values of the primary function (e.g., H_{ti} or E_{ti}) differ only slightly then the mean value of them would be the most reasonable choice for the true value. Otherwise, when the h_{ti}-points are distantly placed then one should seek the global maximum on the indentation primary function to determine the corresponding true value.

4. CONCLUSIONS

In this study, a simple approach to assess stress-strain field (SSF) gradient and divergence from nanoindentation measurement data has been derived and applied in the analysis of the nanoindentation response of a bulk silicon sample. The total, *P′-h,* total elastic, *S′-h,* total plastic, *H′-h*, and elastic normal, *E′-h*, SSF gradients have been revealed as dimensionless functions by the SSF gradient-divergence approach using specific derivatives calculated of the empirically obtained primary indentation functions (load-displacement, *P-h*, stiffness-displacement, *S-h*, hardness-displacement, *H-h*, and elastic modulus-displacement, *E-h*, curves, respectively). In contrast to their corresponding primary functions, the SSF gradients did not contain slowly changing trends determined to some extent by indenter geometry and indentation mode. Instead, relatively weak undulations and peculiarities of the SSF caused by sample heterogeneities, interfaces between mechanically different mediums, phase transformations or other plastic deformation effects could now be observed more clearly and analysed. The traditionally measured averaged datasets describe the indentation response in a somewhat integrated way where the fine undulations can be to a large extent concealed. Therefore, it was important to analyse single indentation test datasets prior to any smoothening and averaging. Further applications of the strain gradient-divergence analysis approach to several steel, glass and fused silica samples, which are chosen as representative materials of bulk solids commonly used as substrates for thin film deposition, are demonstrated in the second part of the present research [10].

The stress-strain gradient approach is not limited to the investigation of bulk solids. The most promising application, in fact, is related to the studies of layered thin film coating structures, where the assessment of the mechanical properties is especially challenging [7], [19], [20]. The influences of the substrate surface are present throughout the thin film sample, which can result in indentation size effects that preclude a precise estimation of the true hardness and true elastic modulus. Furthermore, the thin films can be highly heterogeneous with gradients of changing chemical composition throughout the sample. In such cases, the strain gradient representations can be used to define an analytic criterion for determining the indentation depth at which the apparent values are the closest to the true values: the true mechanical properties should be read out in the most homogeneous regions within the sample, i.e., at the penetration depths where the strain gradient is the closest to zero. Stress-strain gradient representations can also inform about the microstructure of the thin film by revealing a pattern of strain gradient peaks and valleys which

could indicate interfaces between sub-layers of the thin film and relative "in-bulk" zones within the layered thin film structure, respectively.

ACKNOWLEDGEMENTS

The authors express their gratitude to Dr. Roberts Zabels at the Institute of Solid State Physics, University of Latvia for providing the datasets of the nanoindentation and AFM experiments, and Prof. Janis Maniks for encouraging and helpful discussions.

REFERENCES

1. Fischer-Cripps, A. (2004). *Nanoindentation*. New York: Springer-Verlag.
2. Oyen, M.L., & Cook, R.F. (2009). A practical guide for analysis of nanoindentation data. *J. Mech. Behav. Biomed., 2*, 396–407.
3. Guo, Y.B., & Warren, A.W. (2005). Microscale mechanical behavior of the subsurface by finishing processes. *J. Manuf. Sci. Eng.*, *126*, 333–338.
4. Warren, A.W., Guo, Y.B., & Weaver, M.L. (2006). The influence of machining induced residual stress and phase transformation on the measurement of subsurface mechanical behavior using nanoindentation. *Surf. Coat. Tech., 200*, 3459–3467.
5. Michel, J.P., Ivanovska, I.L., Gibbons, M.M., Klug, W.S., Knobler, C.M., Wuite, G.J.L., & Schmid, C.F. (2006). Nanoindentation studies of full and empty viral capsids and the effects of capsid protein mutations on elasticity and strength. *Proc. Natl. Acad. Sci. USA, 103*, 6184–6189.
6. Sangwal, K. (2000). On the reverse indentation size effect and microhardness measurement of solids. *Mater. Chem. Phys., 63*, 145–152.
7. Kanders, U., Kanders, K., Maniks, J., Mitin, V., Kovalenko, V., Nazarovs, P., & Erts, D. (2015). Nanoindentation response analysis of Cu-rich carbon–copper composite films deposited by PVD technique. *Surf. Coat. Tech., 280,* 308–316.
8. Saha, R., & Nix, W.D. (2002). Effects of the substrate on the determination of thin film mechanical properties by nanoindentation. *Acta Mater.*, *50*, 23–38.
9. Manika, I., & Maniks, J. (2008). Effect of substrate hardness and film structure on indentation depth criteria for film hardness testing. *J. Phys. D. Appl. Phys., 41*, 074010.
10. Kanders, U., & Kanders, K. (2017). Nanoindentation response analysis of thin film substrates-II: Strain hardening-softening oscillations in subsurface layer. *Proc. Latv. Acad. Sci. B, 71*.
11. Fleck, N., & Hutchinson, J. (1997). Strain gradient plasticity. *Adv. Appl. Mech., 33*, 295–362.
12. Gao, H., Huang, Y., & Nix, W.D. (1999). Modeling plasticity at the micrometer scale. *Naturwissenschaften*, *86*, 507–515.
13. Johnson, K.L. (1970). The correlation of indentation experiments. *J. Mech. Phys. Solids*, *18*, 115–126.
14. Johnson, K.L. (1985). *Contact Mechanics*. Cambridge: Cambridge University Press.
15. Hay, J.L., Agee, P., & Herbert, E.G. (2010). Continuous stiffness measurement during instrumented indentation testing. *Exp. Techniques, 34*, 86–94.
16. Oliver, W., & Pharr, G. (2004). Measurement of hardness and elastic modulus by instrumented indentation: Advances in understanding and refinements to methodology. *J. Mater. Res.*, *19*, 3–20.

17. Zarudi, I., Zhang, L.C., Cheong, W.C.D., & Yu, T.X. (2005). The difference of phase distributions in silicon after indentation with Berkovich and spherical indenters. *Acta Mater.*, *53*, 4795–4800.
18. Yan, J., Takahashi, H., Gai, X., Harada, H., Tamaki, J., & Kuriyagawa, T. (2006). Load effects on the phase transformation of single-crystal silicon during nanoindentation tests. *Mater. Sci. Eng. A*, *423*, 19–23.
19. Misra, A., Verdier, M., Lu, Y.C., Kung, H., Mitchell, T.E., Nastasi, M., & Embury, J.D. (1998). Structure and mechanical properties of Cu-X (X= Nb, Cr, Ni) nanolayered composites. *Scripta Mater., 39*, 555–560.
20. Maniks, J., Mitin, V., Kanders, U., Kovalenko, V., Nazarovs, P., Baitimirova, M., Meija, R., Zabels, R., Kundzins, K., & Erts, D. (2015). Deformation behavior and interfacial sliding in carbon/copper nanocomposite films deposited by high power DC magnetron sputtering. *Surf. Coat. Tech.*, *276*, 279–285.

VAKUUMA PĀRKLĀJUMU SUBSTRĀTU NANOINDENTĒŠANAS DATU ANALĪZE-I: DEFORMĀCIJAS GRADIENTA-DIVERĢENCES METODE

U. Kanders, K. Kanders

K o p s a v i l k u m s

Nanoindentēšanas metode tiek plaši izmantota mikromehānisku sistēmu mehānisko īpašību pētīšanai, kā, piem., maza izmēra objektu vai maza tilpuma materiālu cietība, Junga modulis, elastības limits vai slodžu izturība, u.c. parametri. Šajā pētījumā ir izstrādāta vienkārša empīriska metode, kā no parauga slogošanas-atslogošanas datiem nanoindentēšanas eksperimentā var izskaitļot indentēšanas radīto deformācijas gradientu un diverģenci. Šādai pieejai ir neaizvietojama praktiska nozīme, kas ļauj daudz drošāk analizēt materiālu cietības un Junga moduļa raksturlīknes atkarībā no indentora iespiešanās dziļuma. Deformācijas gradients un diverģence skaidri norāda uz deformācijas procesu īpatnībām nano-izmēra tilpumos, kas saistīti ar materiālu lokāliem uzkaldināšanas un atkaldināšanas procesiem, piem., masīvu materiālu pievirsmas slānī. Šajā rakstā gradienta-diverģences analīzes metode tika izmantota, lai analizētu masīvu silikona paraugu. Šī pētījuma otrajā daļā (U. Kanders, K. Kanders: Vakuuma pārklājumu substrātu nanoindentēšanas datu analīze-II: Uzkaldināšanas-atkaldināšanas oscilācijas pievirsmas slānī.) šī metode tika izmantota, lai analizētu dažādu tēraudu, stikla un kausēta kvarca masīvu paraugu pievirsmas deformācijas procesus.

09.01.2017.